Diffeomorphic registration with sliding conditions: Application to the registration of lungs CT images.

Laurent Risser, Habib Baluwala and Julia A. Schnabel

Institute of Biomedical Engineering, University of Oxford, Oxford, UK.
{laurent.risser,habib.baluwala,julia.schnabel}@eng.ox.ac.uk *

Abstract. In this paper, we propose a novel diffeomorphic registration method for respiratory motion correction, taking the sliding motion of organs into account. Modelling sliding conditions in image registration has recently gained a strong interest in the medical imaging community. It allows to estimate physiologically realistic deformations at the boundaries of organs like the lungs. This potentially leads to a more accurate registration within the organs. An issue with these algorithms is that they either estimate organ motion within regions of interest only, or they do not ensure the invertibility of the deformations. We propose a strategy to incorporate sliding motion modelling into a piecewise diffeomorphic image registration algorithm inspired by the LogDemons algorithm. Encoding the deformations in velocity fields instead of standard displacement fields ensures the invertibility of the deformations, even at the boundaries where the sliding motion is modelled. We show that our methodology is computationally tractable for serial 3D CT images of the lungs and that it estimates more plausible deformations than by using LDDMM diffeomorphic registration without sliding conditions.

1 Introduction

Sliding motion naturally occurs between the lungs and surrounding structures. This is emphasised in figure 1, where we show the displacement of a vessel within the lungs relative to two ribs. The main efforts to-date in correcting for respiratory motion in lung imaging, as reviewed in [14], use registration based on B-splines [7, 8], thin-plate splines [4, 5], hybrid feature- and intensity-based registration [15] or optical flow or diffusion (demons) type methods [18]. However, none of these methods is able to model non-smooth, discontinuous sliding motion due to organ slippage adequately. For this reason, these methods only register the lungs extracted from the background. A recent approach to biomechanical

* "LR and JAS would like to acknowledge funding from EPSRC EP/H050892/1 and the Cancer Research UK / EPSRC Oxford Cancer Imaging Centre. HB is funded by a Dorothy Hodgkin Postgraduate Award which is a joint sponsorship between EPSRC and Siemens Molecular Imaging (Oxford). We finally want to than the organisers of MICCAI EMPIRE 2010 challenge for the data they gave.

patient-specific respiratory motion modelling is described in [17]. It is however computationally too complex to be used for automated image registration tasks. Recently, [10–12, 19] introduced approaches for direction-dependent regularisation in diffusion-based registration frameworks. Though promising, these methods cannot ensure the invertibiliy of the deformations as the motion is encoded in the displacement fields. Note that an overview state-of-the art techniques for lungs registration is published in [9]

Due to the large amount of respiratory motion, preserving the topology of the deformations can be challenging in pulmonary image registration. To tackle this issue, we propose a novel piecewise diffeomorphic registration algorithm for respiratory motion correction which takes the sliding motion of organs into account. A property of diffeomorphic registration is to mathematically ensures the invertibility and smoothness of the deformations. By using piecewise diffeomorphic registration, we mathematically ensure the invertibility of the deformations in the whole domain. We however allow non-smooth deformations in surfaces representing some organ boundaries. In this context, we perform piecewise diffeomorphic registration by simultaneously taking into account the sliding motion along the lung surface and compensating for deformations occurring within the lungs due to expansion or compression.

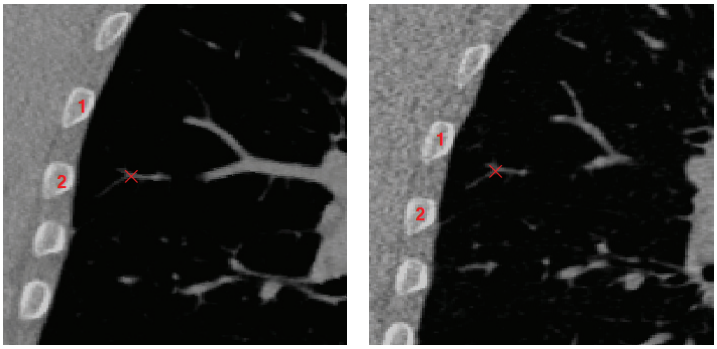

Baseline image Follow-up image

Fig. 1. Illustration of the sliding motion at the lung boundary. The motion of the vessel designated by the red cross and the ribs (1) and (2) show the sliding motion at the lung boundary.

In order to ensure the invertibility of the deformations, we extend the diffeomorphic formalism of the Log-Demons algorithm [6, 16]. We modify the smoothing step of the Log-Demons registration algorithm. Inspired by [10, 12], we separate the contributions of the update velocity fields which are normal and tangent to the surface boundaries, respectively. We then smooth independently the normal contribution in the whole image and the tangent contributions in each region. The regularised update velocity field is then the sum of the smoothed

normal and tangent contributions. The use of a diffeomorphic formalism implies that the source image is deformed during a finite amount of time $t \in [0,1]$ by a velocity field to match the target image. Importantly, the boundaries at which the sliding motion is modelled also move during the time $t \in [0,1]$. As a result, the velocity field is regularized as a function boundaries which depend on time. The diffeomorphism is then necessarily encoded by a time-dependent velocity field, and not a stationary one like in [6, 16]. Details of the algorithm are described in the next section.

2 Diffeomorphic image registration with sliding conditions

2.1 Notations

Let I_S be a source image defined on the spatial domain $\Omega \subset \mathbb{R}^n$ and registered on the target image I_T through the diffeomorphic transformation $\phi_{\mathbf{t}}^{\mathbf{v}}$, $t \in [0,1]$. We construct $\phi_{\mathbf{t}}^{\mathbf{v}}$ using a time-dependent velocity field $\mathbf{v_t}$ and $\frac{\partial}{\partial_t}\phi_{\mathbf{t}}^{\mathbf{v}} = \mathbf{v_t}(\phi_{\mathbf{t}})$, where $\phi_{\mathbf{0}}$ is the identity transformation. The deformed source and the target images at time t are then $I_S \circ (\phi_{\mathbf{t}}^{\mathbf{v}})^{-1}$ and $I_T \circ \phi_{\mathbf{1}}^{\mathbf{v}} \circ (\phi_{\mathbf{t}}^{\mathbf{v}})^{-1}$, respectively. For clarity, we denote J_t^S and J_t^T as these images. Let $M \in \Omega$ be a mask which encodes the labels of different structures in I_S between which sliding conditions are considered. We assume a combination of diffusion and fluid spatial regularisation. The regularisation is then obtained by smoothing vector fields, into the velocity field $\mathbf{v_t}$ or the update velocity field, denoted by $\delta\mathbf{v_t}$, using Gaussian kernels. We denote these Gaussian kernels by G_{σ_d} and G_{σ_f}, where σ_d and σ_f are the standard deviation of the Gaussian kernel for the diffusion and the fluid regularisation, respectively. It is important to note that in the case of diffeomorphic registration, the sliding conditions cannot only be considered at the region boundaries of M since they move with the diffeomorphism $\phi_{\mathbf{t}}^{\mathbf{v}}$. When smoothing $\delta\mathbf{v_t}$ or $\mathbf{v_t}$ for $t \neq 0$, the sliding conditions can be modelled at the regions boundaries in $M_t = M \circ (\phi_{\mathbf{t}}^{\mathbf{v}})^{-1}$. Finally, let Ω_t^k, $k \in [1, \cdots, K]$ be the K regions defined by M_t, and $\partial\Omega_t^k$ denote their boundaries.

2.2 Diffeomorphic Registration Algorithm

In order to embed sliding conditions in a diffeomorphic registration setting, we develop an extension of the LogDemons algorithm which makes use of time-dependent velocity fields, instead of stationary ones like in [16]. This extension requires more computational resources than [16] but allows the proper treatment of the sliding motion, as previously explained. In [16] and here, the optimal velocity field $\tilde{\mathbf{v}}$ is obtained by minimising $\tilde{\mathbf{v}} = \arg\min_{\mathbf{v}} E(\mathbf{v}, \mathbf{v^c})$, where the energy E is defined as:

$$E(\mathbf{v}, \mathbf{v_c}) = \frac{1}{\lambda_i^2}||J_1^T - J_1^S||_{L^2}^2 + \frac{1}{\lambda_x^2}\int_0^1 ||\mathbf{v_t} - \mathbf{v_t^c}||_{L^2}^2 dt + \frac{1}{\lambda_d^2}\int_0^1 ||\nabla\mathbf{v_t}||_{L^2}^2 dt \quad (1)$$

In Eq. 1, $\mathbf{v^c}$ encodes an intermediate diffeomorphism $\phi_{\mathbf{t}}^{\mathbf{v^c}}$ (so-called correspondence), which is matching the two images without considering the regularity of the transformation. Discussions about setting appropriate weights λ_i, λ_x, λ_d are developed in [6]. In practice, the optimal velocity field $\tilde{v}$ is obtained by computing $\mathbf{v}$ and $\mathbf{v^c}$ alternatingly: First, an update velocity field $\delta\mathbf{v_t}$ is estimated and used to compute the time-dependent velocity field $\mathbf{v_t^c}$. By referring to the so-called *Thirion forces*, the update $\delta\mathbf{v_t}$ is defined as:

$$\delta\mathbf{v_t}(\mathbf{x}) = -\frac{J_t^S - J_t^T}{||\mathbf{G}(\mathbf{x})||^2 + \lambda_i^2/\lambda_x^2}\mathbf{G}(\mathbf{x}) \tag{2}$$

where $\mathbf{G}(\mathbf{x}) = \nabla J_t^S(\mathbf{x})$ is the gradient of the deformed source image intensities, $\lambda_i = J_t^S - J_t^T$, and λ_x controls the maximum update length per iteration. Prior to the composition, $\delta\mathbf{v}$ may be smoothed (fluid like regularisation). Then $\mathbf{v_t}$ is updated to from a smoothed velocity field $\mathbf{v_t^c}$ (diffusion like regularisation). Contrary to [16], we solve this problem using time-dependent velocity field and we incorporate sliding conditions in the smoothing steps. The algorithm may be described as follows:

1: $\mathbf{v_t} = \mathbf{0}$, $\forall t \in [0,1]$.
2: $\phi_{\mathbf{t}}^{\mathbf{v}} = \mathbf{Id}$, $\forall t \in [0,1]$.
3: **while** not convergence **do**
4: Compute the update velocity field $\delta\mathbf{v_t}$ using Eq. 2, $\forall t \in [0,1]$.
5: Smooth $\delta\mathbf{v_t}$, $\forall t \in [0,1]$ (fluid regularisation).
6: Compute the correspondence velocity: $\mathbf{v_t^c} = \mathbf{v_t} + \delta\mathbf{v_t}$, $\forall t \in [0,1]$.
7: Smooth $\mathbf{v_t^c}$, $\forall t \in [0,1]$ (diffusion regularisation).
8: Set $\mathbf{v_t}$ as equal to $\mathbf{v_t^c}$, $\forall t \in [0,1]$.
9: Compute $\phi^{\mathbf{v}}$ using $\mathbf{v}$
10: **end while**

While our extension of [16] presents similarities with the LDDMM registration algorithm of [3] and the popular method of [2], the key difference is the formulation for estimating the updates, leading to different estimation estimates. In particular, our proposed registration algorithm is not designed to estimate geodesics between the registered images, like in [3]. The deformations we estimate cannot therefore be represented using initial momenta. Another difference with both [2, 3] is that in addition to performing fluid regularisation, the diffusion regularisation allows to interpolate the deformations in regions with low intensities gradients, and not only at the observed structures boundaries. This property can be of great interest in image registration in general, especially compared with [3], which relates the amplitude of the smoothing kernel to the size of the structures and not the image, and therefore prohibits the use of standard multi-resolution strategies. Finally, the link between Eq. 1 and our algorithm is still not entirely clear. We however ensure the estimation of piecewise diffeomorphic transformations and show the usability of our strategy on real 3D images in section 3.

2.3 Nearest region boundary estimation

When registering two images with sliding conditions at organs boundaries, we aim to register the organ boundaries, while simultaneously smoothing the deformations within each organ independently. When regularising the velocity field $\delta\mathbf{v_t}$, we therefore need to isolate the contributions of $\delta\mathbf{v_t}$ which are normal and tangent to the region boundaries, in order to smooth them separately. This requires the estimation of the vector map $\mathbf{B}(\mathbf{x}) = \mathbf{x}\tilde{\mathbf{x}}$, where $\tilde{\mathbf{x}}$ is the closest point to $\mathbf{x}$ on $\partial\Omega_t^k$ according to an Euclidian distance metric.

Our strategy to estimate $\mathbf{B}$ is based on the fact that the region labels are encoded by integer values in the mask M and that trilinear interpolation is performed to estimate the grey levels of M_t. Hence, a region boundary in M_t may not necessarily be defined as the coordinate between two voxels of different integer intensities. If the point $\mathbf{x}$ of M_t has a non-integer value, the gradient $\mathbf{g}(\mathbf{x}) = \nabla M_t(\mathbf{x})$ is estimated at a sub-voxel accuracy. The different integer intensities l_1 and l_2 which are obtained on $M_t(\mathbf{x} + \tau\mathbf{g}(\mathbf{x}))$, for the smallest values of $\tau \in \mathbb{R}$, are considered as the labels of the regions surrounding $\mathbf{x}$. We then define the distance between $\mathbf{x}$ and the boundary $\partial\Omega_t^k$ as the value of τ for which $M_t(\mathbf{x} + \tau\mathbf{g}(\mathbf{x})) = (l_1 + l_2)/2$. After estimation of the values of $\mathbf{B}$ in the 6-neighbourhood of $\partial\Omega_t^k$, the information about the closest boundaries is iteratively propagated in Ω.

2.4 Fluid-like spatial regularisation with sliding conditions

After estimating the vector map $\mathbf{B}$, which points to the nearest points of the boundaries $\partial\Omega_t^k$ from each point in the domain Ω, we perform the fluid-like spatial regularisation as follows:

1. For each point $\mathbf{x}$ in Ω and not on a boundary $\partial\Omega_t^k$, we decompose $\delta\mathbf{v_t}(\mathbf{x})$ into its normal and tangent components to the nearest boundary, respectively denoted by $\delta\mathbf{v_t^N}(\mathbf{x})$ and $\delta\mathbf{v_t^T}(\mathbf{x})$. The normal component is computed as $\delta\mathbf{v_t^N}(\mathbf{x}) = (\hat{\mathbf{B}}(\mathbf{x}) \cdot \delta\mathbf{v_t}(\mathbf{x}))\hat{\mathbf{B}}(\mathbf{x})$, where $\hat{\mathbf{B}}(\mathbf{x}) = \mathbf{B}(\mathbf{x})/||\mathbf{B}(\mathbf{x})||$ and $(\mathbf{A} \cdot \mathbf{B})$ is the scalar product between the vectors $\mathbf{A}$ and $\mathbf{B}$. The tangent component is $\delta\mathbf{v_t^T}(\mathbf{x}) = \delta\mathbf{v_t}(\mathbf{x}) - \delta\mathbf{v_t^N}(\mathbf{x})$.
2. The vector field $\delta\mathbf{v_t^N}$ is homogeneously smoothed in Ω using isotropic diffusion.
3. Independently in each region Ω_t^k, we smooth the values of $\delta\mathbf{v_t^N}$ using homogeneous isotropic diffusion and by considering Neumann boundary conditions at the domain boundaries. More specifically, we impose null derivatives at each region boundary.
4. After smoothing the different components of $\delta\mathbf{v_t}$, this velocity field is recomposed as $\delta\mathbf{v_t}(\mathbf{x}) = \delta\mathbf{v_t^N}(\mathbf{x}) + \delta\mathbf{v_t^T}(\mathbf{x})$, $\forall x$.

At each point, the contributions of the deformations tangent to the region surface, which are related to the sliding motion, are therefore only regularised within the considered regions. The normal contributions, which not only participate in the displacement of the structures within the regions, but also in the

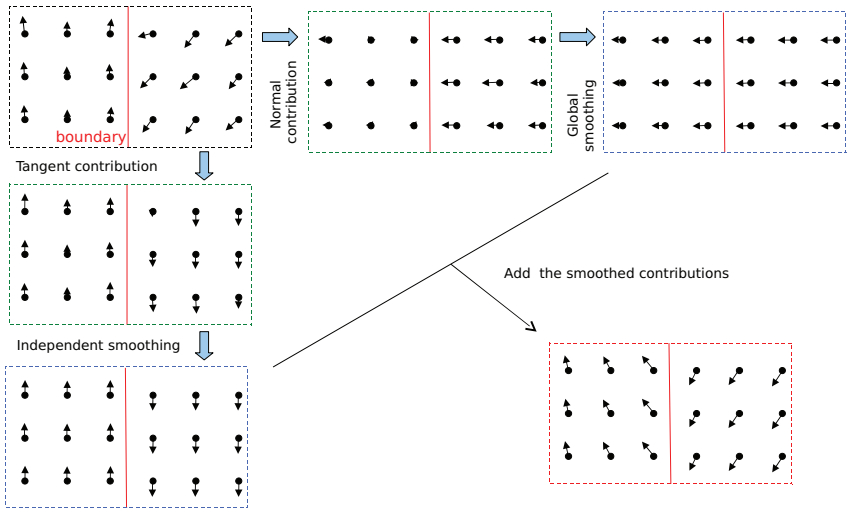

Fig. 2. Smoothing of the update vector field $\delta\mathbf{v_t}(\mathbf{x})$ to perform fluid-like regularisation. The red line represents the boundary at which the discontinuity is modelled.

displacement of the structures boundaries, are smoothed in the whole image. This strategy is illustrated in figure 2.

2.5 Diffusion-like spatial regularisation with sliding conditions

In our methodology, we only smooth the forces at the boundaries $\partial\Omega_t^k$ in the fluid-like regularisation step. The only purpose of the fluid-like regularisation is to diffuse the deformations in the regions of Ω having low intensity gradients. Homogeneous, isotropic diffusion of the vector fields $\mathbf{v_t}$ is then performed independently in the different regions Ω_t^k. Unlike the von Neumann boundary conditions used for the fluid-like regularisation, we use here Dirichlet boundary conditions. Our aim is to preserve the deformations estimated at the region boundaries, hence no smoothing is performed at the regions boundaries.

3 Evaluation

In our tests, we compare the proposed piecewise diffeomorphic algorithm with the LDDMM registration algorithm of [3] on a pair of phantom images and real 3D pulmonary CT images:

– The phantom dataset was generated using the 4D NURBS-based Cardiac-Torso (NCAT phantom) toolkit developed by [13]. The 4D NCAT phantom

is a realistic and flexible simulation tool for generating CT volumes and modelling cardiac and respiratory motion. Two images of $96 \times 96 \times 96$ voxels representing the lungs at the end of expiration and at the end of inhalation were generated.

– The 3D CT image pair is the 8^{th} data set of the MICCAI EMPIRE 2010 challenge [1, 9]. This challenge proposes an amount of 30 lungs image pairs to register and uses an advanced protocol to evaluate the quality of the registration. Here, we only assess the usability of our registration algorithm and discuss key differences observed when considering or not sliding conditions. Among the 30 data sets, we use the 8^{th} one as it has a large field of view around the lungs and it requires relatively large deformations. The target (fixed) image was resampled at half resolution ($1.5 \times 1.5 \times 1.4$mm) and the source (moving) image was not resampled ($0.75 \times 0.75 \times 0.7$mm). All computations were performed in the target image space ($219 \times 157 \times 196$ voxels). A rigid alignment of the images was first performed. At each iteration of the non-rigid registration algorithm, the source and target images are compared by composing the rigid and non-rigid deformations, so the source image is only resampled one time.

Sliding motion of the lungs against the chest wall takes place across the pleura during breathing. The pleural cavity is a body cavity that surrounds the lungs and allows the pleurae to slide effortlessly against each other during ventilation. Since the pleura surrounds the lungs the sliding motion does not take place, exactly at the lung surface but at a distance of one to two pixels away from the boundary. It is important to take this mechanical behaviour into consideration as it forms an essential part of the physiological breathing motion of the lungs. Figures 3 and 4 respectively illustrate the matchings and the displacement fields obtained on the NCAT dataset. Figures 5 and 6 also illustrate the matchings and the displacement fields obtained on the patient 08 of the EMPIRE challenge. Note that, contrary to the displacement fields of Fig. 6 (d-e), those of Fig. 6 (b-c) incorporate the rigid alignment between the images. In Fig. 6 (b-c), the regions in blue represent a large displacements while those in red represent small displacements. Table 1 gives quantitative results.

As shown in Figures 3 and 5 the matching quality is equivalently improved using non-rigid registration with or without sliding conditions compared to a rigid registration. After rigid registration the lungs overlap is about 90% in the NCAT and EMPIRE data sets. This overlap is more than 98% after non-rigid registration. This is also quantified, in table 1, where the sum of squared difference between I_T and $I_S \circ \Phi$ is equivalently lower using LDDMM and piecewise diffeomorphic registration than using rigid registration. The mutual information, where a lower value represents a better matching, shows the same trend.

Figures 4 and 6 however show that modelling sliding conditions allows to estimate more realistic deformations than by using a homogeneous regularisation like in the LDDMM algorithm. Due to the lack of significant features in some parts of the images, the similarity term of the minimised energy can't have enough weight compared to the regularisation term in order to estimate

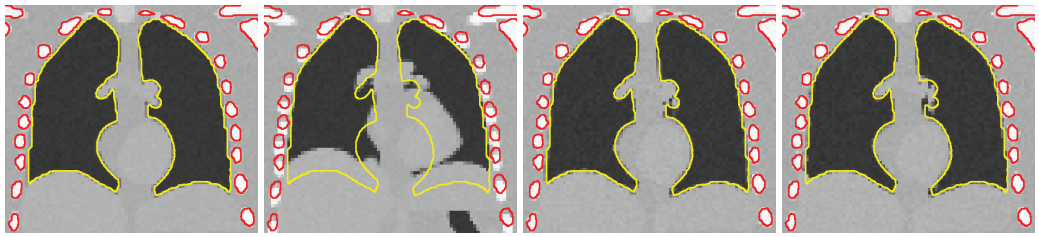

Fig. 3. Registration of the NCAT images using LDDMM and the proposed piecewise diffeomorphic registration algorithm (disc). The isolines represent the lung and bone boundaries in I_T.

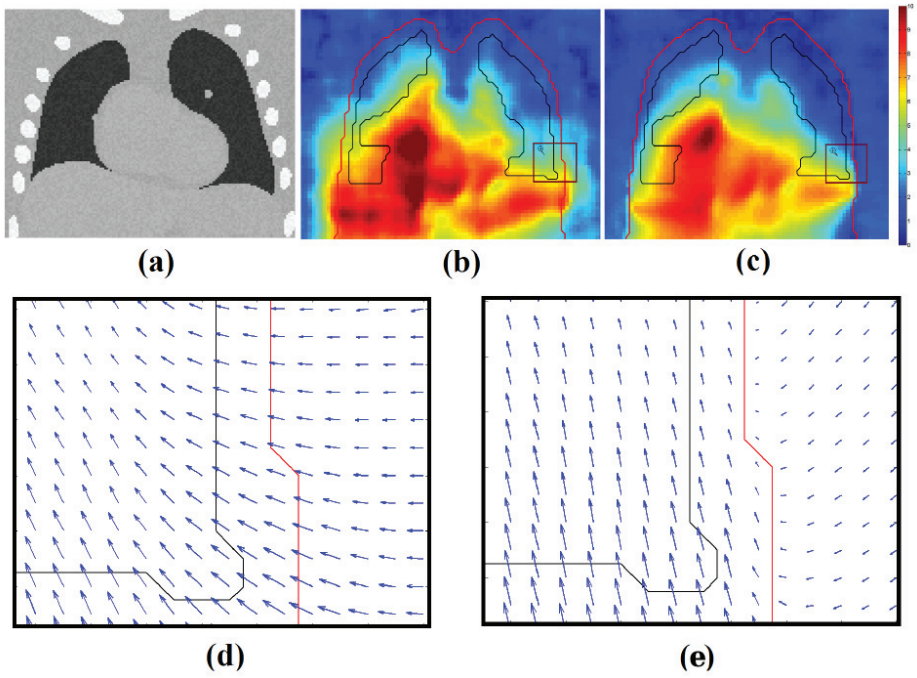

Fig. 4. Deformations estimated on the NCAT data. **(a):** Coronal view of the 3D source image **(b) and (c):** Amplitude of the deformations. **(d) and (e):** 2D projection of the displacement field in a ROI. The black curves represent the lung boundaries and the red ones the location of the discontinuities. **(b) and (d):** LDDMM. **(c) and (e):** Piecewise diffeomorphic registration.

of natural deformations. Modelling explicitly the sliding motion in the spatial regularisation appears as mandatory in this case (see Figure 5).

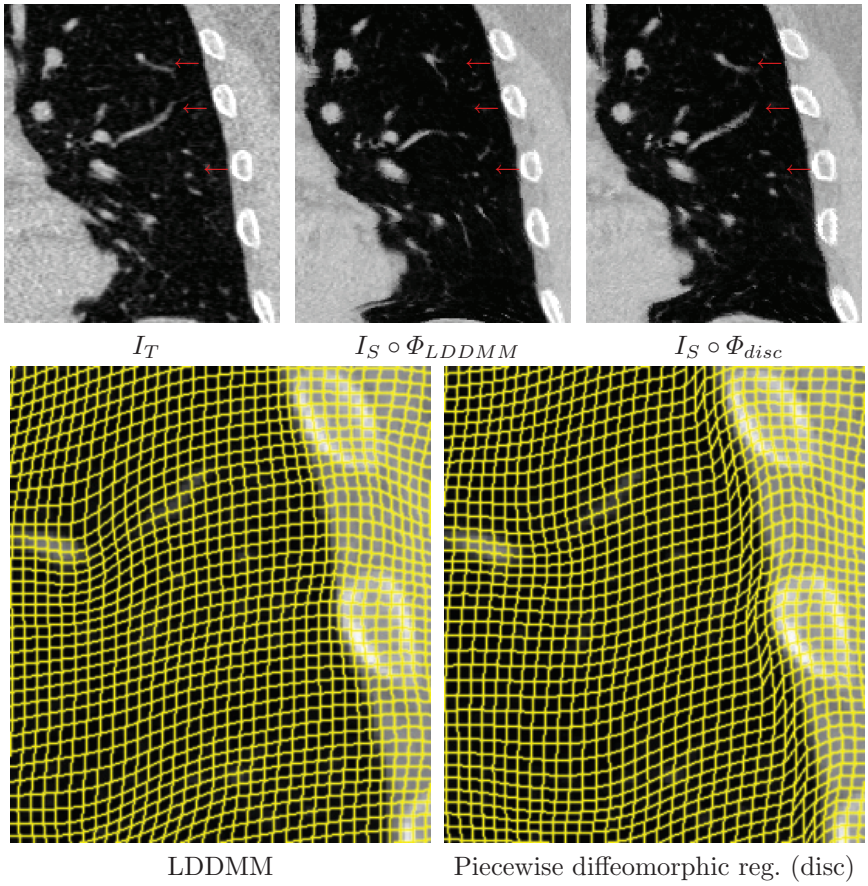

Fig. 5. (Top) ROI in the target image and the deformed source image after LDDMM and disc. Arrows clearly show a better vessel alignment using disc. **(Bottom)** Grids deformed by the transformations estimated using LDDMM and disc showing the sliding motion at the lung surface.

Table 1 shows that with or without sliding motion, the average determinant of Jacobians is $1 \pm 3\%$ in the bones, which is physiologically plausible since the bones are not subject to compression or expansion. The corresponding standard deviations are however lower when the sliding motion is modelled. This motion is therefore more plausible, as also shown in the deformed grids of Figure 5. Note that in the discontinuities look slightly fuzzy do to the fact that the images were registered at a half resolution/ It is interesting to note that, for a similar matching quality, less deformations are required to register the whole images using the sliding motion. This is quantified by lower standard deviations of the determinant of Jacobians in the whole images, and also visible in the top row of

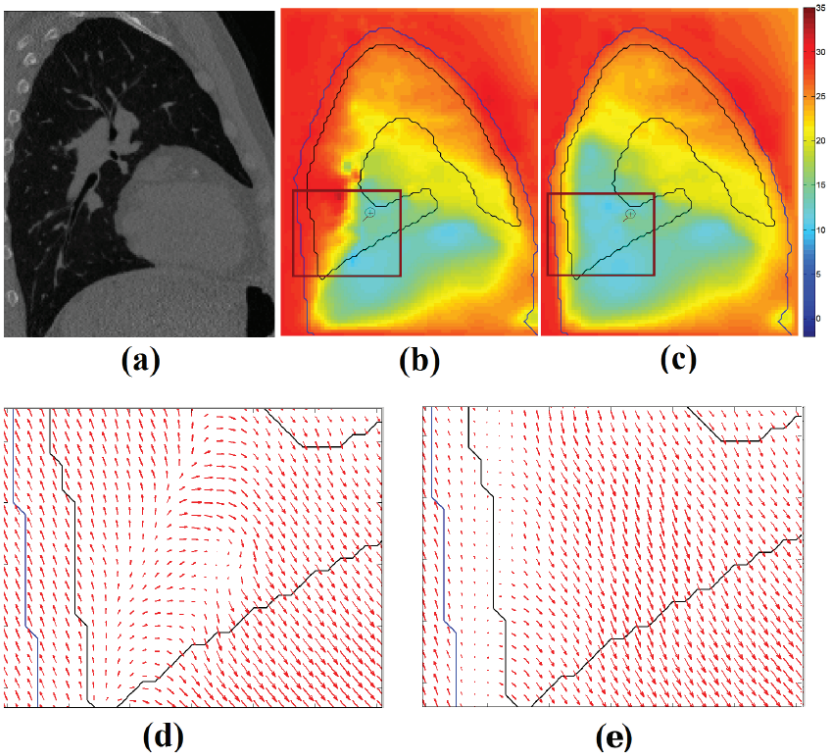

Fig. 6. Deformations estimated on the patient 08 of the EMPIRE dataset. **(a):** Slice of the 3D source image **(b) and (c):** Amplitude of the deformations. **(d) and (e):** 2D projection of the displacement field in a ROI. The black curves represent the lung boundaries and blue one the location of the discontinuities. **(b) and (d):** LDDMM. **(c) and (e):** Piecewise diffeomorphic registration.

figure 4 which presents a larger magnitude in (b). Another important result is shown in the first row of figure 5: The motion of some vessels within the lungs is only correctly estimated by taking into account a sliding motion between the lungs and surrounding structures. Note that the matching of these vessels could be even further improved with less spatial regularisation. This however would generate non-plausible deformations with little interpolation between the structures observed in the images. We finally estimated the deformations invertibility by measuring the number of voxels with negative determinant of the Jacobians. No negative Jacobians were computed using by LDDMM and piecewise diffeomorphic registration. Most of them are localised at the region boundaries, where the sliding motion is modelled, and are close to zero.

Table 1. Quality of the rigid, LDDMM and piecewise diffeomorphic registration (disc) in the NCAT images and the patient 08 of the EMPIRE dataset. **(From left to right)** Sum of square differences (SSD) and mutual information between the registered images. Standard deviation of the determinant of Jacobian (J) in the whole deformation (total), and average and standard deviation of the determinant of Jacobian within the bones (bones).

		SSD	**MI**	**std($\|J\|$) total**	**av($\|J\|$) bones**	**std($\|J\|$) bones**
NCAT	Rigid	0.17	-0.73	0	1	0
	LDDMM	0.072	-1.16	0.45	1.018	0.34
	disc	0.077	-1.15	0.30	1.027	0.18
Pat. 08	Rigid	0.037	-0.51	0	1	0
	LDDMM	0.018	-0.83	0.36	0.993	0.17
	disc	0.018	-0.81	0.28	0.997	0.12

4 Conclusion

We have presented a novel diffeomorphic registration method which addresses the problem of sliding conditions and boundary displacements at which these conditions are estimated. The use of a registration algorithm in which the deformations are embedded in a time-dependent velocity field allows to model large deformations with locally strong discontinuities, while mathematically preserving the invertibility of the deformations. In practice, a negligible amount of negative Jacobians is observed in the deformation but their value is close to zero. Importantly, the sliding conditions gave us the opportunity to realistically model the physiological motion at the lung boundary, leading to potentially more accurate registration within the lungs. This is particularly true in regions where the images present few features and an advanced model is required to regularise the deformations. Future work will deal with further developments of the mathematical justification of the proposed model. In particular, linking the regularisation strategy and the minimised energy would be of high interest from a theoretical point of view. Further tests of our method on the MICCAI'10 Empire dataset will also be performed. We expect that the proposed strategy should also be helpful for a wider range of applications, where sliding conditions are needed, like in the heart or the liver for instance.

References

1. http://empire10.isi.uu.nl
2. Avants, B.B., Epstein, C.L., Grossman, M., Gee, J.C.: Symmetric diffeomorphic image registration with cross-correlation: Evaluating automated labeling of elderly and neurodegenerative brain. Medical Image Analysis 12, 26–41 (2008)

3. Beg, F.M., Miller, M.I., Trouvé, A., Younes, L.: Computing large deformation metric mappings via geodesic flows of diffeomorphisms. International Journal of Computer Vision 61(2), 139–157 (February 2005)
4. Coselmon, M.M., Balter, J.M., McShan, D.L., Kessler, M.L.: Mutual information based CT registration of the lung at exhale and inhale breathing states using thin-plate splines. Medical Physics 31(11), 2942–2948 (2004)
5. Li, B., Christensen, G.E., Hoffman, E.A., McLennan, G., Reinhardt, J.M.: Establishing a normative atlas of the human lung: Intersubject warping and registration of volumetric ct images. Academic Radiology 10(3), 255 – 265 (2003)
6. Mansi, T., Pennec, X., Sermesant, M., Delingette, H., Ayache, N.: iLogDemons: A demons-based registration algorithm for tracking incompressible elastic biological tissues. International Journal of Computer Vision 92(1), 92–111 (2011)
7. Mattes, D., Haynor, D., Vesselle, H., Lewellen, T., Eubank, W.: Pet-ct image registration in the chest using free-form deformations. IEEE Trans. Med. Imaging 22(1), 120 –128 (2003)
8. McClelland, J.R., Blackall, J.M., Tarte, S., Chandler, A.C., Hughes, S., Ahmad, S., Landau, D.B., Hawkes, D.J.: A continuous 4D motion model from multiple respiratory cycles for use in lung radiotherapy. Medical Physics 33(9), 3348–3358 (2006)
9. Murphy, K., Van Ginneken, B., Reinhardt, J.M., Kabus, S., Ding, K., Deng, X., Pluim, J.P.W., et. al: Evaluation of registration methods on thoracic ct: The empire10 challenge. IEEE Trans. Med. Imaging 25(4), 385 –405 (2011)
10. Pace, D.F., Enquobahrie, A., Yang, H., Aylward, S.R., Niethammer, M.: Deformable image registration of sliding organs using anisotropic diffusive regularization. In: Proceedings of ISBI. pp. 407–413 (2011)
11. Ruan, D., Esedoglu, S., Fessler, J.: Discriminative sliding preserving regularization in medical image registration. In: Proceedings of IEEE ISBI. pp. 430 –433 (2009)
12. Schmidt-Richberg, A., Ehrhardt, J., Werner, R., Handels, H.: Slipping objects in image registration: improved motion field estimation with direction-dependent regularization. In: Proceedings of MICCAI. pp. 755–762 (2009)
13. Segars, W.P.: Development of a new dynamic NURBS-based cardiac-torso (NCAT) phantom. Ph.D. thesis, The University of North Carolina (2001)
14. Sluimer, I., Schilham, A., Prokop, M., van Ginneken, B.: Computer analysis of computed tomography scans of the lung: a survey. IEEE Trans. Med. Imaging 25(4), 385 –405 (2006)
15. Stewart, C.V., Lee, Y.L., Tsai, C.L.: An uncertainty-driven hybrid of intensity-based and feature-based registration with application to retinal and lung ct images. In: Proceedings of MICCAI. vol. 3216, pp. 870–877 (2004)
16. Vercauteren, T., Pennec, X., Perchant, A., Ayache, N.: Symmetric log-domain diffeomorphic registration: A demons-based approach. In: Proceedings of MICCAI. pp. 754–761 (2008)
17. Werner, R., Ehrhardt, J., Schmidt, R., Handels, H.: Patient-specific finite element modeling of respiratory lung motion using 4D CT image data. Medical Physics 36(5), 1500–1511 (2009)
18. Werner, R., Ehrhardt, J., Schmidt-Richberg, A., Heiß, A., Handels, H.: Estimation of motion fields by non-linear registration for local lung motion analysis in 4D CT image data. International Journal of Computer Assisted Radiology and Surgery 5(6), 595–605 (2010)
19. Yin, Y., Hoffman, E., Lin, C.L.: Lung lobar slippage assessed with the aid of image registration. In: Proceedings of MICCAI. vol. 6362, pp. 578–585 (2010)